08

Investigation of the effect of oxygen partial pressure on the phase composition of copper oxide nanoparticles by vacuum arc synthesis

© A.V. Ushakov,[1,2] I.V. Karpov,[1,2] L.Yu. Fedorov,[1,2] E.A. Goncharova,[1,2] M.V. Brungardt,[1] V.G. Demin[1]

[1] Siberian Federal University,
660041 Krasnoyarsk, Russia
[2] rasnoyarsk Scientific Center of the Siberian Branch of the Russian Academy of Sciences,
660036 Krasnoyarsk, Russia
e-mail: sfu-unesco@mail.ru

Received May 25, 2021
Revised August 9, 2021
Accepted August 10, 2021

Copper oxide nanoparticles were obtained in the plasma of a low-pressure arc discharge. The effect of the partial pressure of oxygen (10−40%) on the physical properties of the deposited nanoparticles has been studied. X-ray diffraction analysis shows that the cubic structure of Cu_2O changes to monoclinic CuO with increasing O_2 pressure. The results of Raman spectroscopy further confirmed the phase variations of copper-based oxide nanoparticles. X-ray photoelectron spectroscopy confirmed the change in the binding energy in the oxidation state of nanoparticles. The optical band gap of the deposited Cu_2O is 2.12 eV, while that of CuO is 1.79−1.82 eV.

Keywords: vacuum arc, oxides, nanoparticles, plasma-chemical reactions.

DOI: 10.21883/TP.2022.15.55268.157-21

Introduction

The use of nanoparticles (NP) of various materials and their chemical compounds offers significant advantages due to their size and unique physical and chemical properties. In almost all cases, the synthesis method should produce nanoparticles with a narrow size distribution, minimal particle size, chemical purity and hence their specific properties [1–5].

In recent years, the synthesis and applications of Cu_2O and CuO with controlled size and morphology continue to be intensively investigated [6]. CuO is a more stable oxide than Cu_2O, due to the greater stability of the Cu (II) ions in the environment. Despite this, both CuO and Cu_2O, due to their low band gap width, high optical absorption and catalytic activity, have wide practical applications, the most important of which are photovoltaic systems [7], gas sensors [8], various heterogeneous catalysts [9] In addition, copper oxides are non-toxic [10], have low cost and the possibility of a large variety of morphological forms in the synthesis [11]. One of the most efficient methods of producing nano-disperse materials remains gas-phase synthesis and, in particular, the method of evaporation−condensation [12-14].

The aim of this work is to investigate the process of vacuum arc synthesis of copper oxide at different values of partial oxygen pressure, to study the effect of this parameter on the phase composition of the formed nanoparticles, and to characterize the synthesized products by spectroscopic methods.

1. Experimental procedure

The experimental setup and the dependence of powder properties on atomization conditions are discussed in detail in [15–18]. Copper oxide nanoparticles were deposited on a stainless steel substrate by arc sputtering using a M0 copper cathode. The plasma-forming gas used was argon, which was fed through an evaporator and generated a base pressure of 80 Pa in the chamber. Oxygen was used as the reaction gas. The synthesis of nanoparticles was investigated at partial oxygen pressures of 10, 20, 30 and 40%. Oxygen was fed into the reactor in such a way as to form a homogeneous envelope around the plasma torch. Powder production was carried out for 15 min, and after heating the chamber (3 min), the powder deposited during synthesis was removed from the substrate with a plastic scraper.

The phase composition of the obtained samples was investigated by X-ray powder diffraction on Bruker D8 Advance equipment in CuK_α mono-chromatized radiation ($\lambda = 0.15406$ nm). The samples placed in the diffractometer cuvette were powder scraped off the substrate after sputtering. Such a powder has a random orientation of individual nanoparticles and their agglomerates. Quantitative structural-phase analysis of the diffraction patterns was carried out with the full-profile analysis software Powder Cell 2.4. The average lattice parameters were determined by the Scherrer method from diffraction peaks using the equation $d = K\lambda/\beta\cos\theta$. PDF-4+ databases from the International Centre for Diffraction Data (ICDD) were used to identify radiographs.

Raman studies were carried out with a Bruker RFS 100/S Raman spectrometer. A Nd−YAG laser with $\lambda = 532$ nm at an output power of 8 mW in the range of 50−800 cm^{-1} was used as the excitation source.

X-ray photoelectron spectroscopy studies were carried out on an ultra-high vacuum photoelectron spectrometer, PHOIBOS 150MCD9, SPECS Gmbh, when excited by AlK_α X-ray tube radiation. Casa XPS software was used for quantitative analysis.

Optical measurements were made on a Perkin Elmer Lambda 950 spectrophotometer and transmission spectra were obtained. Samples for the study were prepared by co-pressing tablets with potassium bromide and stripped nanoparticles (in a 1 : 100 ratio) with a diameter of 13 mm and a thickness of ~ 0.55 mm.

2. Results and discussion

Fig. 1 shows X-ray diffraction patterns of copper oxide NP at various partial pressures of O_2 from 10 to 40%. The above diffraction patterns show the formation of three different copper oxide phases as the partial pressure of O_2 varies. Three major diffraction peaks at 36.5°, 42.4° and 61.4° were obtained for the Cu_2O [PDF–4+ № 78–2076] phase at 10% O_2 partial pressure, which correspond to crystal reflection planes (111), (200) and (220). The diffraction peaks of mixed Cu_4O_3 and CuO phases appear at 35.7° and 38.6°, which correspond to crystal planes (202) for the paramelaconite phase Cu_4O_3 [PDF-4+ № 04-007-2184] and (111) for CuO phase, respectively. When the O_2 pressure is increased to 20%, the corresponding Cu_2O diffraction peaks disappear. A further increase in the O_2 partial pressure up to 40% leads to the formation of mono-phase CuO particles, and the observed diffraction peaks at 35.6°, 38.6° and 48.8° confirm the orientation of crystal planes (002), (111) and (-202) for the CuO phase [PDF-4+ № 45-0937].

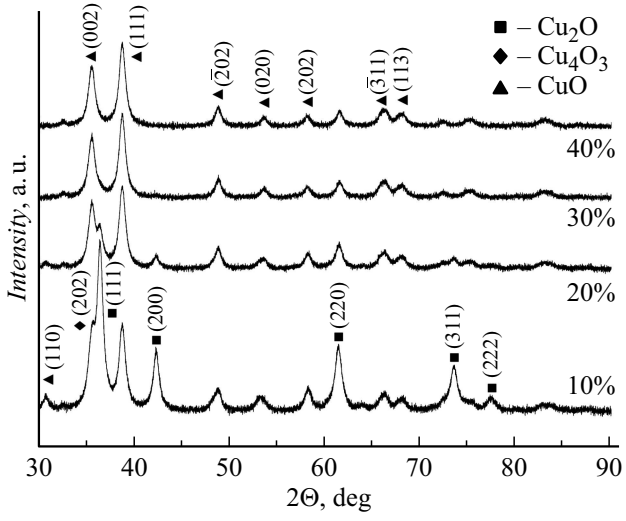

Figure 1. X-ray diffraction patterns of copper oxide NP deposited at different partial pressures of oxygen.

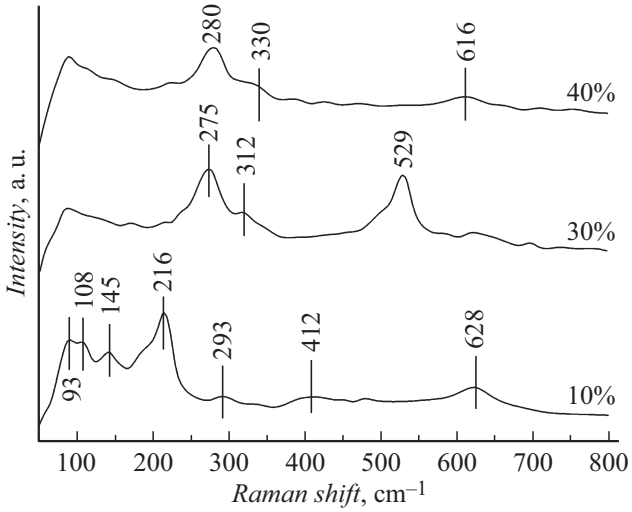

Figure 2. Raman spectra of copper oxide NP deposited at different partial pressures of oxygen.

Using the Debye−Sherrer equation, the coherent scattering regions (CSR) of Cu_2O and CuO nanoparticles were calculated. The resulting CSR values, identified with the crystallite size, were virtually unchanged with increasing O_2 pressure and were 12 nm. The percentage of oxygen had no effect on the CSR values. Here, the value of the total pressure plays a decisive role, as can be seen in more detail in previous works [15,17–19]. In addition, these papers compare the results calculated from X-ray radiographs of the average size of the CSR with the results of transmission electron microscopy. Among the CuO NP, the best crystallinity is shown by those deposited at a pressure of 40% O_2.

Raman spectrometry is an additional method for determining the phase structure of NP. The influence of the partial pressures of O_2 on the structure formation of the deposited NP was further investigated by means of Raman light scattering analysis (Fig. 2). The most dominant peak occurs at 216 cm^{-1} for NP deposited at 10% O_2 pressure, which corresponds to the second order Raman mode ($2\Gamma_{15}^-$) Cu_2O. The peak at 145 cm^{-1} can be attributed to Raman scattering of light on symmetry phonons F_{1u}. The peak at 108 cm^{-1} is attributed to the inactive Raman mode. The weak peak at 412 cm^{-1} corresponds to a four-phononon mode ($3\Gamma_{15}- + \Gamma_{25}-$). In addition, the weak peak located at 293 cm^{-1} is associated with an overtone mode of second order symmetry A_{2u}. The moderate peak at 628 cm^{-1} refers to the active IR mode. A small peak at 93 cm^{-1} was found for defects, resonance excitation and nonstoichiometry in Cu_2O NP. These observed modes of oscillation confirm the presence of Cu_2O phase with a cubic structure in the spatial group Oh^4 with two formulaic units per lattice cell. The Raman spectra of NP deposited at 30% O_2 partial pressure show characteristic peaks at 275, 320 and 529 cm^{-1}. The strong peak at 275 cm^{-1} with a peak on the shoulder at 320 cm^{-1} corresponds to the A_g and B_g^1 CuO

Raman modes, respectively. Another peak is observed at 529 m^{-1}, which is attributed to the Raman mode A_{1g} of the paramelaconite Cu_4O_3 phase. Consequently, this confirms the formation of the CuO and Cu_4O_3 two-phase system. This agrees well with the results of X-ray diffraction. NP obtained at 40% O_2 partial pressure show three peaks at 280, 330 and 616 cm^{-1}, corresponding to the A_g, B_g^1 and B_g^2 CuO Raman scattering mode respectively. According to the results, CuO belongs to the spatial group C_{2h}^6 with a monoclinic structure of two molecules per primitive cell. The combination of X-ray diffraction analysis and Raman studies directly establishes the phase composition existing in the deposited copper oxide NP as a function of the partial pressure O_2.

The synthesis of single phase NP copper oxide is challenging because the change in partial pressure has a very small window (about 10%) to reach a particular phase. This is because the free path length of the atomized copper atoms decreases as the O_2 partial pressure increases, which in turn reduces the NP deposition rate [20–23].

The X-ray photoelectron spectroscopy (XPS) method was used to confirm the chemical state of the constituent elements in the prepared samples. Only three elements are detected on the NP surface, namely Cu, O and C. Table 1 shows the relative atomic concentrations of copper, oxygen and carbon calculated from overview spectra of samples (not shown in the work) synthesized at different values of partial oxygen pressure. Carbon is present at the C1*s* peak position (284.8 eV) — inevitably adsorbed by samples from the atmosphere, or directly in the vacuum oil process.

The XPS method allows to work only with the surface layer, with the majority of the signal (95%) coming from a depth of less than 8 nm from the surface. In this regard, atomic percentage data is insufficient to analyze the phase composition of the samples as the result is affected by any rearrangement of atoms leading to compounds on the surface of nanoparticles, so XPS spectra with narrow scanning of Cu2*p* and O1*s* axis levels were studied to establish the phase composition of oxide nanoparticles (Fig. 3).

XPS spectra of the Cu2*p*level histone spectra show that the Cu2$p_{3/2}$ and Cu2$p_{1/2}$ photoelectron peaks are observed at 932.2 and 952.3 eV respectively for the Cu_2O phase-dominated NP (obtained at 10% O_2). Similarly, the same peaks are found at 933.7 and 953.6 eV for the CuO NP

Table 1. Relative atomic concentration of copper, oxygen and carbon calculated from survey spectra

Partial oxygen pressure, %	Element content, at.%		
	Cu	O	C
10	40.7	28.1	31.2
20	38.2	25.1	36.7
30	37.1	27.1	35.8
40	35.1	34.0	30.9

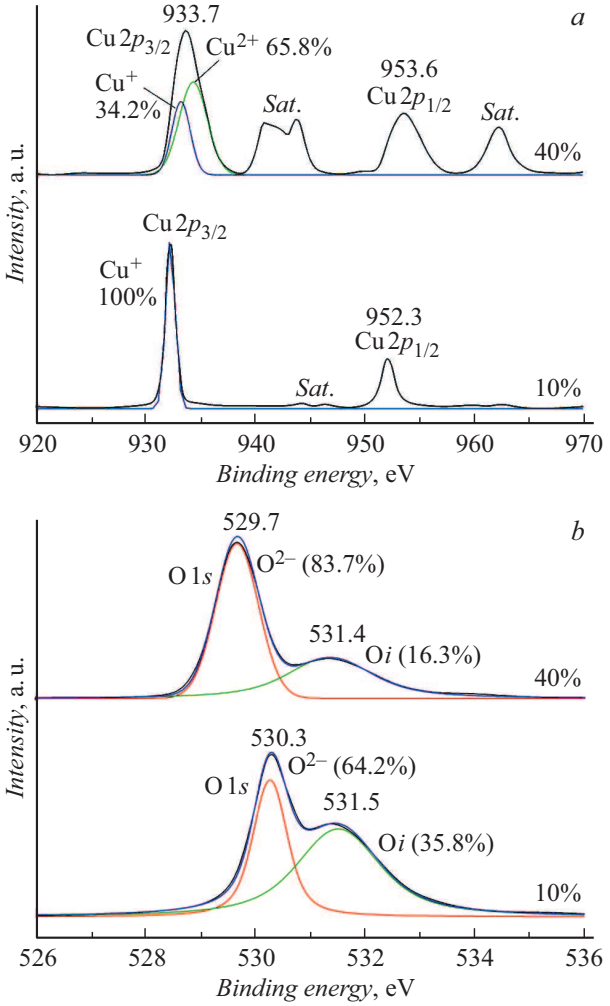

Figure 3. Narrow scan XPS spectra of Cu2*p* (*a*) and O1*s* (*b*) Cu oxide NP deposited at different oxygen partial pressures.

phase (obtained at 40% O_2). Cu^+ ions in $Cu_{\{2\}}O$ NP have a high intense peak at position $2p_{3/2}$ compared to Cu^{2+} ions in CuO NP. In addition to the main communication energy peaks, satellite peaks are also observed. This is due to the different types of particles that bind Cu and O, or the oxidation degrees of Cu^+ and Cu^{2+}. For the Cu_2O NP, some small weak satellite peaks on the higher binding energy side in the range 944–946 eV are also observed. Similarly, CuO NP have strong and broad satellite peaks located between 940 and 944 eV, corresponding to the doublet oxidation states of Cu^{2+}. Alongside this, a single satellite peak at 962.3 eV is also observed for the CuO phase.

The Cu2$p_{3/2}$ peak was found to shift towards higher binding energies from 932.2 to 933.7 eV when the partial pressure of O_2 increases from 10 to 40%. This indicates a change in the oxidation degree of Cu from Cu^+ to Cu^{2+}. The changes in binding energy are confirmed by the Cu2$p_{3/2}$ peaks observed for both the Cu_2O NP and the single-phase CuO NP.

From the O1s spectrum of deposited NP it can be seen that the main O1s peak is detected at 530.3 and 529.7 eV

Table 2. Quantitative analysis of XPS spectra of Cu2$p_{3/2}$ and O1s

Conditions obtaining	Photovoltaic the bonding	Energy Value line, eV	Percentage content, %	State of the atom
40% O_2	Cu2$p_{3/2}$	932.7	34.2	Cu+
	934.6	65.8	Cu^{2+}	
	O1s	530.3	83.7	O_{2-}
	Shoulder peak	531.5	16.3	Oi
10% O_2	Cu2$p_{3/2}$	932.7	100	Cu^{+}
	O1s	529.7	64.2	O_{2-}
	Shoulder peak	531.4	35.8	Oi

for copper oxide NP synthesized at 10 and 40% respectively. In addition, shoulder peaks are also observed at 531.5 and 531.4 eV. The O1s peak was found to shift slightly towards a lower binding energy from 530.3 to 529.7 eV when the partial pressure of O_2 increases from 10 to 40%. The lower binding energy peaks can be attributed to the Cu and O binding components in copper oxides, whereas the peaks with higher binding energy shoulders are due to chemisorbed oxygen (Oi) on the surface.

Table 2 shows the results of quantitative analysis of the XPS spectra of Cu2$p_{3/2}$ and O1s levels. From the presented data, the presence of oxygen atoms in the Cu^{+} state in the samples obtained at O_2 40% partial pressure seems to indicate the presence of Cu_2O phase in the nanoparticle surface layer.

The XPS results are complementary to the X-ray diffraction, Raman and energy dispersive analysis results discussed earlier and are also in good agreement with the data presented in [24–27].

Transmittance spectra of deposited NP at different partial pressures of O_2 are shown in Fig. 4.

The optical transmittance of deposited nanoparticles was found to depend only on their phase composition determined by the O_2 partial pressure value during synthesis. It should be noted that in all modes, the average NP diameter is maintained at around 12 nm. The transmittance decreases as the partial pressure of O_2 increases. In particular, particles deposited at 10% O_2 partial pressure have, due to lack of O_2, a high average transmittance — about 80% in the near-IR region. NP, deposited at 40% O_2 partial pressure, show an average transmittance of — 60%. The transmittance of Cu_2O samples decreases dramatically from wavelengths below 600 nm. Similarly, the transmission spectra of CuO have an absorption edge with a critical wavelength of around 700 nm. All of the resulting NP have the absorption capacity of visible light. As for the small fluctuations in the spectrum of copper oxide obtained at an oxygen partial pressure of 10%, it seems that they can be explained by the difference in refraction indices between the oxide nanoparticles and the substrate [28].

Numerous studies of Cu_2O oxides (see, for example, [29,30]) have shown that they are characterized by direct interzone transitions. As for CuO, optical absorption studies show that Cu(II) oxides are semiconductors with an energy gap in the range $\sim 1-2$ eV (see, for example, [31]). However, from a theoretical point of view, the calculation of the electronic structure of CuO is a difficult task [32] and no reproducible results for exact values of the band gap as well as the nature of the band gap transition have been published. In the work [33], the band structure diagrams of different copper oxide phases were plotted and the calculated values of the band gap width for the indirect transition in CuO were obtained. However, the authors of this paper separately note good agreement with experiment for Cu_2O and discrepancies for CuO.

In this paper, however, the band gap widths of both oxides are determined by the Tauck parabolic zone model using the relation,

$$\alpha h\nu = A(h\nu - Eg)^{n/2},$$

where A — proportional constant, n — depends on the nature of the transition ($n = 1$ for a direct resolved transition), ν — energy of the incident photon, α — absorption factor, and E_g — width of the optical band gap. Here the absorption coefficient α is directly related to the transmittance (T) and diameter (d) of the NP. The absorption coefficient α can be estimated from the following relation [34]:

$$\alpha = \frac{1}{d}\ln\left[\frac{1}{T}\right],$$

where T — transmittance, d — average NP diameter.

Fig. 4, *b* shows Tauck graph ($(\alpha h\nu)^2$ vs photon energy h *nu*) of deposited NP at different partial pressures of O_2.

The intersection of the line with the $h\nu$-axis at zero determines the band gap width (E_g) for the resolved optical transition. Nanoparticle samples with the predominant Cu_2O phase (deposited at 10% O_2 partial pressure) show a band gap width value of 2.12 eV. The band gap width of CuO particles deposited at 40% was 1.82 eV. The values

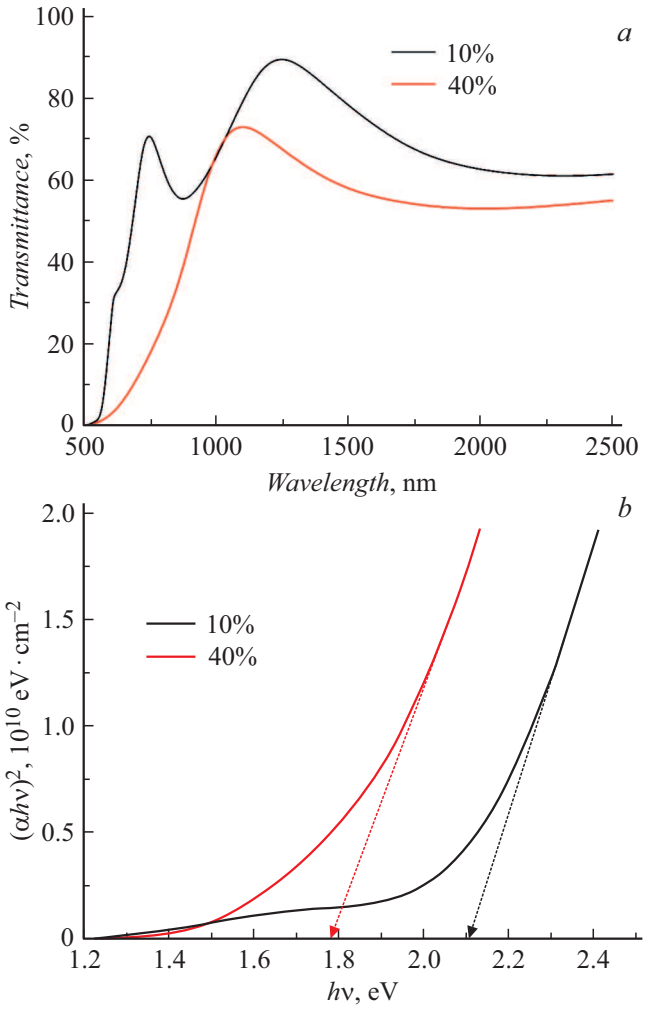

Figure 4. Transmission spectra (*a*) and Tauck's graph (*b*) of copper oxide NP at different partial pressures of oxygen.

obtained are in good agreement with the results presented in [35,36].

Conclusion

Thus, the effect of partial oxygen pressure in the gas mixture of the plasma chemical reactor on the ratio of the forming crystalline phases of copper oxide nanoparticles was studied. A complex of X-ray and spectroscopic methods of investigation confirmed the variations of the phase composition of the synthesized oxide nanoparticles depending on the partial pressure of oxygen. With increase in O_2 concentration, the nanoparticle structure is transformed from Cu_2O and Cu_3O_4 to CuO monophase. The photoelectron spectra show, firstly, a strong contamination of the nanoparticles surface with adsorbed carbon, which may be caused by the oil evacuation system of the processing plant, and secondly, the presence of particles of phase composition Cu_2O in the CuO phase surface layer as a result of insufficient oxygen saturation of copper clusters formed by arc evaporation. The results of the band gap width determination for the resolved optical transition of Cu_2O and CuO nanoparticles, being 2.12 eV and 1.82 eV respectively, are in good agreement with the literature data. However, determining the nature of the band gap and the band gap width for CuO nanoparticles requires further research, as conventional methods in the framework of density functional theory cannot describe this compound as a semiconductor. At the same time, the results of such research could bring the practical use of copper oxides in photovoltaic devices closer.

Funding

The study was supported by a grant from the Russian Science Foundation (Project № 20-19-00021). Optical research was carried out at the Siberian Federal University's Collaborative Use Centre with the support of the Russian Ministry of Science and Higher Education State Assignment (FSRZ-2020-0011).

Conflict of interest

The authors declare that they have no conflict of interest.

References

[1] C.M. Niemeyer. Angew. Chem. Int. Ed., **40** (22), 4128 (2010). DOI: 10.1002/1521-3773(20011119)40:22
[2] W. Ma, L. Xu, A.F. de Moura, X. Wu, H. Kuang, C. Xu, N.A. Kotov. Chemical Rev., **117** (12), 8041 (2017). DOI: 10.1021/acs.chemrev.6b00755
[3] L. Mohammed, H.G. Gomaa, D. Ragab, J. Zhu. Particuology, **30**, 1 (2017). DOI: 10.1016/j.partic.2016.06.001
[4] W. Xiang, Y. Liu, J. Yao, R. Sun. Physica E: Low-dimensional Syst., Nanostruct., **97**, 363 (2018). DOI: 10.1016/j.physe.2017.12.016
[5] S.P. Jahromi, A. Pandikumar, B.T. Goh, Y.S. Lim, W.J. Basirun, H.N. Lim, N.M. Huang. RSC Adv., **5** (18), 14010 (2015). DOI: 10.1039/C4RA16776G
[6] P. Lignier, R. Bellabarba, R.P.R. Tooze. Chem. Soc. Rev., **41**, 1708 (2012). DOI: 10.1039/C1CS15223H
[7] Y. Abdu, A.O. Musa. J. Pure. Appl. Sci., **2**, 8 (2009).
[8] K.J. Choi, H.W. Jang. *Sensors* (Basel, Switzerland, 2010), v. 10, p. 4083. DOI: 10.3390/s100404083
[9] M.B. Gawande, A. Goswami, F.-X. Felpin, T. Asefa, X. Huang, R. Silva, X. Zou, R. Zboril, R.S. Varma. Chem. Rev., **116**, 3722 (2016). DOI: 10.1021/acs.chemrev.5b00482
[10] O. Bondarenko, K. Juganson, A. Ivask, K. Kasemets, M. Mortimer, A. Kahru. Archives of Toxicology, **87** (7), 1181 (2013). DOI: 10.1007/s00204-013-1079-4
[11] Q. Zhang, K. Zhang, D. Xu, G. Yang, H. Huang, F. Nie, C. Liu, S. Yang. Progress Mater. Sci., **60**, 208 (2014). DOI: 10.1016/j.pmatsci.2013.09.003
[15] F. Gao, X.J. Liu, J.S. Zhang, M.Z. Song, N. Li. J. Appl. Phys., **111**, 084507 (2012). DOI: 10.1063/1.4704382
[13] Q. Yang, Z. GuO, X.H. Zhou, J.T. Zou, S.H. Liang. Mater. Lett., **153**, 128 (2015). DOI: 10.1016/j.matlet.2015.04.045

[14] A.H. Jayatissa, K. Guo, A.C. Jayasuriya. Appl. Surf. Sci., **255**, 9474 (2009). DOI: 10.1016/j.apsusc.2009.07.072
[15] I.V. Karpov, A.V. Ushakov, A.A. Lepeshev, L.Yu. Fedorov. Tech. Phys., **62** (1), 168 (2017). DOI: 10.1134/S106378421701011X
[16] A.V. Ushakov, I.V. Karpov, A.A. Lepeshev. J. Superconductivity and Novel Magnetism, **30** (12), 3351 (2017). DOI: 10.1007/s10948-017-4311-2
[17] A.V. Ushakov, I.V. Karpov, A.A. Lepeshev, L.Yu. Fedorov. Int. J. Nanosci., **16** (4), 1750001 (2017). DOI: 10.1142/S0219581X17500016
[18] I.V. Karpov, A.V. Ushakov, V.G. Demin, A.A. Shaihadinov, A.I. Demchenko, L.Yu. Fedorov, E.A. Goncharova, A.K. Abkaryan. J. Magnetism and Magnetic Materials, **490**, 165492 (2019). DOI: 10.1016/j.jmmm.2019.165492
[19] A.V. Uschakov, I.V. Karpov, A.A. Lepeshev, M.I. Petrov. Vacuum, **133**, 25 (2016). DOI: 10.1016/j.vacuum.2016.08.007
[20] X. Hu, F. Gao, Y. Xiang, H. Wu, X. Zheng, J. Jiang, J. Li, H. Yang, S. Liu. Mater. Lett., **176**, 282 (2016). DOI: 10.1016/j.matlet.2016.04.055
[21] S. Cui, E.C. Mattson, G. Lu, C. Hirschmugl, M. Gajdardziska-Josifovska, J. Chen. J. Nanopart Res., **14**, 744 (2012). DOI: 10.1007/s11051-012-0744-5
[22] S. Sério, M.E. Melo Jorge, M.J.P. Maneira, Y. Nunes. Mater. Chem. Phys., **126**, 73 (2011). DOI: 10.1016/j.matchemphys.2010.12.008
[23] E. Turgut, Ö. Coban, S. Sarıtas, S. Tüzemen, M. Yıldırım, E. Gür. Appl. Surf. Sci., **435**, 880 (2018). DOI: 10.1016/j.apsusc.2017.11.133
[24] Y. Alajlani, F. Placido, A. Barlow, H.O. Chu, S. Song, S.U. Rahman., R. De Bold, D. Gibson. Vacuum, **144**, 217 (2017). DOI: 10.1016/j.vacuum.2017.08.005
[25] G. Murdoch, M. Greiner, M. Helander, Z. Wang, Z. Lu. Appl. Phys. Lett., **93** (8), 318 (2008). DOI: 10.1063/1.2966140
[26] T. Gaewdang, N. Wongcharoen. IOP Conf. Ser.: Mater. Sci. Eng., **211**, 012025 (2017). DOI: 10.1088/1757-899X/211/1/012025
[27] A. Jilani, M.S. Abdel-Wahab, M.H.D. Othman, V. Sajith, A. Alsharie. Optik, **144**, 207 (2017). DOI: 10.1016/j.ijleo.2017.06.075
[28] S. Cho. Met. Mater. Int., **19** (6) 1327 (2013). DOI: 10.1007/s12540-013-6030-y
[29] D.A. Kudryashov, A.S. Gudovskikh, A.V. Babichev, A.V. Filimonov, A.M. Mozharov, V.F. Agekyan, E.V. Borisov, A.Yu. Serov, N.G. Filosofov. Semiconductors, **51** (1), 110 (2017). DOI: 10.1134/S1063782617010110
[30] A.B. Gordienko1, Yu.N. Zhuravlev, D.G. Fedorov. Phys. Solid State, **49** (2), 223 (2007). DOI: 10.1134/S1063783407020072
[31] D. Chauhan, V.R. Satsangi, S. Dass, R. Shrivastav. Bull. Mater. Sci., **29** (7), 709 (2007).
[32] B.K. Meyer, A. Polity, D. Reppin, M. Becker, P. Hering, P.J. Klar, Th. Sander, C. Reindl, J. Benz, M. Eickhoff, C. Heiliger, M. Heinemann, J. Bläsing, A. Krost, S. Shokovets, C. Müller, C. Ronning. Phys. Stat. Sol. B, **249** (8), 1487 (2012). DOI: 10.1002/pssb.201248128
[33] M. Heinemann, B. Eifert, C. Heiliger. Phys. Rev. B, **87**, 115111 (2013). DOI: 10.1103/PhysRevB.87.115111
[34] M.T.S. Nair, L. Guerrero, O.L. Arenas, P.K. Nair. Appl. Surf. Sci., **150** (1−4), 143 (1999). DOI: 10.1016/S0169-4332(99)00239-1
[35] S.C. Ray. Solar Energy Materials and Solar Cells, **68** (3−4), 307 (2001). DOI: 10.1016/S0927-0248(00)00364-0
[36] A.Y. Oral, E. Menşur, M.H. Aslan, E. Başaran. Mater. Chem. Phys., **83** (1), 140 (2004). DOI: 10.1016/j.matchemphys.2003.09.015